

Crop, Soil, and Geological Mapping from Digitized Multispectral Satellite Photography

P. E. Anuta
S. J. Kristof
D. W. Levandowski
T. L. Phillips
R. B. MacDonald

Crop, Soil, and Geological Mapping from
Digitized Multispectral Satellite Photography¹

by

P. E. Anuta
S. J. Kristof
D. W. Levandowski
T. L. Phillips
R. B. MacDonald

Laboratory for Applications of Remote Sensing
Purdue University
Lafayette, Indiana

1. INTRODUCTION

Multispectral photography offers a means of measuring the spectral variations in reflected energy from a scene in addition to the spatial and panchromatic tonal measurements obtained from conventional photography. Color and color infrared are the most common forms of multispectral photography. Multiple camera and multilens camera systems employing different film-filter combinations can sense many spectral bands over the range of film sensitivity of approximately .4-.9 micrometers.

A study of digitized multispectral satellite photography was conducted to seek answers to the following two questions: (1) What are the data handling problems and requirements of converting photographic density measurements to a usable digital form; (2) What surface features can be distinguished using multispectral data taken at satellite altitudes. The results of this study include the digitization of three multiband black and white photographs and a color infrared photograph the conversion of the results of digitization to a useful digital form, and several data analysis experiments.

The NASA Apollo 9 mission carried two multispectral photographic sensors.² One consisted of three cameras with black and white film and filter combinations which sensed reflected energy in approximately the .48-.61, .59-.71 and .68-.89 micrometer wavelength bands. The other sensor was a single camera exposing color infrared film, which senses approximately the same bands. Details of the film sensors are presented in Table I. The Imperial Valley, California, was selected as a test site because of the generally low cloud cover over the area and the diversity of ground features, e.g., agricultural areas, desert, mountains. At the time of the mission, extensive ground truth was collected in the Imperial Valley by the University of Michigan³ to enable detailed study of problems related to remote sensing from satellite altitudes. A photographic print of the Apollo 9 frame studied is presented in Figure 1a.

¹This work was supported by the National Aeronautics and Space Administration Grant Number NGL15-005-112 and U. S. Department of Agriculture Contract 12-14-100-10292(20).

²Kaltenbach, J. L., "Apollo 9 Multispectral Photographic Information," NASA TM X-1957, April 1970.

³Spansail, N. et al., "Imperial Valley Ground Truth for Apollo 9 Overflight of March 1969," University of Michigan.

Recent analysis of this photography by Wiegand⁴ et al. produced good results for surface features such as sugar beets and salt flats. Three categories of surface features in the southern California region were studied here: crops, soils and geological features. The analysis described consists of several steps which fall into three major phases.

- data preprocessing
- training class and signature analysis
- automatic classification and result evaluation

Phase 1 includes microdensitometry and color separation of the film, analog to digital conversion, data registration and formatting. Phase 2 and 3 compose an iterative process in which training classes are updated based on classification results obtained from the previous training area, and the process continues until satisfactory results are achieved.

The analysis conducted used digital techniques throughout. This approach allows a wide variety of analysis and display methods to be used in writing and executing the appropriate program for a digital computer.

The paper first discusses the data preprocessing operations which were carried out. Analysis of the data on two levels is then discussed. A large scale or "global" study is performed to determine the spectral signatures of green vegetation, soil, rocks, water, clouds, and other general surface covers (section 5). Then the crop (section 6), soil (section 7), and geological (section 8) classes are studied to determine what features can be discriminated in these categories.

2. PHOTOGRAPHY AS A SENSOR OF SCENE REFLECTANCE

Photographic materials can be viewed as chemical detectors of electromagnetic energy over a limited portion of the spectrum. Electromagnetic energy from the sun is reflected by the scene and collected by the camera-lens system. The amount of energy reaching the film is a function of the sun's energy spectrum, scene bi-directional reflectance, atmospheric attenuation and scattering, lens distortions and filter effects. The exposure of the film is a function of energy reaching it, exposure time, aperture and emulsion characteristics. Variability in all of these parameters is in addition to the scene variability due to different spectral responses of the same class of interest.

The silver halide emulsion of the film is transformed by exposure to the light energy which produces increasing density after development. The relationship between exposure and density is approximately logarithmic, and film sensitivity is described by the well-known $D \log E$ curve. Over the linear portion of the curve the relationship between density and exposure is of the form $D = a + b \cdot (\log E)$. The shape of the $D \log E$ curve can be determined by photographing a step-calibration wedge containing several steps of known exposure variation.

Measurement of film density is facilitated by the wide variety of densitometers available today. A densitometer measures the fraction of light transmitted through the film. This quantity is called transmittance: T . Density is defined as the base 10 logarithm of the inverse of the transmittance:

$$D = \log \frac{1}{T} \text{ or } D = \log \frac{I_0}{I_t}$$

⁴Wiegand, C. L., Leamer, R. W., Gerbermann, A. H., "Crop Species and Soil Condition Discrimination on Ektachrome Infrared Apollo 9 Imagery," USDA, Weslaco, Texas.

where I_o is the incident light and I_t is the transmitted light. The density of the Apollo 9 transparencies studied were measured using a precision rotating drum microdensitometer.* The densities were converted to electrical form, sampled and converted to an eight-bit binary number. The sampling resolution used was approximately .001 inch which resulted in a sampling-ground resolution at nadir of about 200 feet. The estimated resolution of the Apollo 9 photography is approximately 350 feet at nadir and increases to over 750 feet at the edge of the frame. Sampling at 200 feet insures that resolution error is not introduced due to sampling and is large enough that grain effects do not cause extreme noise problems. The digitized density samples were recorded on magnetic tape for computer processing. The 70 mm frames sampled at .001 inch produce about 4.5×10^6 samples.

The three multispectral black and white transparencies were scanned using white light. The color infrared transparency was scanned sequentially using blue, green, and red filters and no filter in the white light path. Thus seven representations of the frame were obtained on tape resulting in a total of over 30 million density readings. A computer gray scale printout of the white light scan of the color infrared frame is presented in Figure 1b. The microdensitometer was adjusted so that the density range of the film covered most of the dynamic range of the instrument.

Surface feature classification was conducted using both multispectral black and white data and color separation data from the color infrared film. The comparison between multispectral and multibase sensors was made to determine the relative merit of the two for the case reported in Section 6. If equal or superior results could be obtained from color film, then the added expense and registration problem associated with the multispectral black and white approach could be avoided.

3. DATA PREPROCESSING

The individual scans were stored as separate data sets on tape. In order to analyze this data using multispectral pattern recognition programs, each of the scans must be stored in such a manner that each scene point is in geometric coincidence in all bands or channels. This image registration problem has been studied at LARS^{5,6} and a software system has been developed to register or "overlay" multiple images of the same scene. This system was used to combine the individual scans onto one tape with the image points stored in such a manner that any ground point can be addressed by a line-and-column coordinate pair and a channel pointer. The data channels and their associated wavelength bands are given in Table II. An IBM System 360 Model 44 computer was available for the analysis.

The calibration operations which can be performed on film data are of two forms:

1. Sensor calibration
2. Scene reflectance calibration

Sensor calibration determines non-linear relationship between film density and incoming radiation, removes the off-axis response reduction, compensates for obliqueness in the image, etc. Scene reflectance calibration relates scene reflectance to the film density resulting from the exposure. Relatively accurate sensor calibration can be achieved by using, for example, calibrated step wedges for exposure calibration and applying known off-axis correction factors. The fall-off

*The film was scanned by Optronics International, Chelmsford, Massachusetts, and Fairchild Space and Defense Systems, Syosset, New York. The cooperation of these two firms is greatly appreciated.

⁵Anuta, P. E., "Digital Registration of Multispectral Video Imagery," SPIE Journal, Vol. 7, No. 6, September 1969.

⁶Anuta, P. E., "Spatial Registration of Multispectral and Multitemporal Digital Imagery Using Fast Fourier Transform Techniques," IEEE Transactions of Geoscience Electronics, Volume GE-5, No. 4, October 1970.

in sensitivity as a function of off-axial position in the scene is approximately as a $\cos^4\theta$ function where θ is the look angle from the principal axis. This effect can be compensated for by dividing the measurements by this function. These are the two major densitometric distortions in photography, and removing them greatly improves the quality of the data. The missing link is the relationship between exposure and scene reflectance. No simple method is available for calibrating scene reflectance, however. Two general approaches can be taken:⁷ (1) determine the incident light energy at the target and the reflected energy at the camera and compute the reflectance; (2) place calibration panels having known reflectance curves in the scene and use the resulting film density for the panels as calibration references. The second method is generally preferred.

No reflectance calibration references were available for the study reported here, and the classification analysis proceeded on the assumption that the separability of the classes of interest could be predicted from the uncalibrated relative scene-reflectance measurements obtained from the photography.

4. TRAINING PROCEDURES FOR THE PATTERN CLASSIFIER

The spectral properties of reflected radiation from a scene can be used to identify the nature or category of objects in the scene. This process is known as a multispectral pattern recognition. The spatial or temporal properties of scene objects can also be used for identification. Alphabetic character recognition is the classic example of pattern recognition using spatial features. Pattern recognition using spectral or temporal data is a relatively new discipline, and the Apollo 9 experiment was one of the first space systems to carry multispectral sensors. There are three major problems which must be addressed when attempting multispectral pattern recognition:

1. Separability of classes of interest
2. Variability of the characteristics of the classes over the domain of the measurements
3. Uniqueness of the spectral characteristics of these classes

The work reported here addresses the first two questions. The uniqueness of the classes over a large area is a complex problem and is the subject of current research at LARS.

Multispectral pattern recognition techniques have recently been applied to automatic remote sensing of crop, soil, geological, and hydrological surface features using data from low altitude airborne multispectral sensors.⁸ The availability of multiband and color infrared photography from the Apollo 9 mission has enabled these same techniques to be tested on data gathered at satellite altitudes.

Several methods are available for studying imagery to determine separable classes in given data. The statistical multispectral pattern analyzer of LARSYSAA (see Reference 8) developed at LARS supplies several methods of class selection. The system can compute the multidimensional first and second order statistics for up to 30 wavelength bands. These statistics are printed out in the form of histograms, correlation matrices, and coincident 1-sigma spectral plots. Any of these forms can be used to group data areas having similar spectral responses. This system also includes a divergence analyzer which can be used to compute the pairwise separability between all classes. The analyzer can also be used to select the optimum set of wavelength bands to be used for classifications based on this

⁷Silvestro, Frank B., "Multispectral Photographic Determination of Reflectance," Photogrammetric Engineering, Vol. 35, No. 3, March 1969.

⁸Fu, K. S., Landgrebe, D. A., Phillips, T. L., "Information Processing of Remotely Sensed Agricultural Data," Proceedings of the IEEE, Vol. 57, No. 4, pp. 639-653, April 1969.

divergence criteria. Another method of class separation utilizes clustering techniques to group image points around cluster centers in multidimensional space in such a way that the overall variance for the resulting sets is minimized.

All surface features to be analyzed are identified by first printing out a gray scale picture on the computer line printer. The gray tones in the original picture are reproduced by a selected set of print chain characters, i.e., blank for very white and M for very dark. Line and column coordinates, which identify uniquely each point in the scene, are printed along the edges of the computer-generated picture. Areas to be studied are specified by their line and column coordinates punched on cards. These cards are read by the analysis program, and the statistical algorithms are applied to the data. The output is inspected manually and the selected data is modified until a satisfactory training set is arrived at. Then a final set of mean and correlation matrices is generated for use by the pattern classifier. This training procedure was applied to each task of recognizing crop, soil and geological features as well as to a synoptic recognition task.

5. SYNOPTIC ANALYSIS OF TOTAL FRAME

A synoptic feature-analysis was made on a global scale over the entire 10,000 square mile area of the frame to develop a computer-derived map of the following features: clouds, cloud shadow, water, rock, bare soil, sand, green vegetation, and salt flats. Training areas were selected by visual inspection of the gray scale pictorial printouts and large photographic prints of the film transparencies. The training areas chosen displayed varieties of surface features in several categories; clustering was then used to define subclasses in these areas. For example, the Imperial Valley produced the green vegetation and bare soil training, the desert region east of the Valley produced the sand and alluvium samples, and mountain areas near the Colorado River were used for rock-type samples. The first and second order multidimensional statistics were then computed using the statistics processor of LARSYSAA. Figure 2 shows the relative spectral reflectance levels for each of the synoptic or global classes considered, along with those for the crop classes to be discussed. These values were obtained from the film density values measured by the film scanner. The analog-to-digital conversion processes and densitometry scale the density measurements to a range of 0 to 255. This range is inverted in the computer so that maximum density is represented by 0 and zero density is represented by 255. Thus, the values in Figure 2 are proportional to scene reflectance; however, the exact relationship is not known.

Classification was performed on the total frame using the LARSYSAA classifier, and the computer-generated surface-feature map obtained is presented in Figure 3. The classification accuracy achieved can not be specified since the only ground truth available was for the NASA test site in the central Imperial Valley. A good estimate of classifier performance can be obtained by simply comparing visually the classification result with areas of known surface cover in the photograph of Figure 1a. Areas of water, bare soil, and green vegetation are readily apparent, and the rock outcrops shown compare closely with a geological map of the area. Overall classification accuracy was judged to be very good. Clouds, cloud shadow, green vegetation, water, sand and alluvium are apparently readily identified by the classifier. The soils, soil-rock mixture, and rock types tend to be confused, but, as stated, precise evaluation was not possible for this experiment. To better evaluate the performance of the classification process much more detailed classification analysis was performed on small test sites.

6. CROP TYPE IDENTIFICATION EXPERIMENTS

The two areas in the central Imperial Valley where extensive ground truth was taken by the University of Michigan are denoted 15A "Dogwood Road" and 15D "McCabe Road". Both of these areas are located within the heavy rectangular border seen in the lower left of Figure 1b. Figure 4a is a computer-generated reproduction of test area 15A, and Figure 4b contains area 15D.

Annotated scanner display prints supplied by the University of Michigan were used to locate the agricultural fields in the computer pictorial printouts. Line and column coordinates of the fields in areas 15A and 15D were identified and punched on cards. The film density data and the field coordinate cards were input into LARSYSAA, and histograms and statistics were computed and printed for each field. Certain crop types such as carrots, lettuce, and onions have very high

percentages of soil background and were present in very small number. An adequate statistical sample could not be obtained for these classes; thus they were deleted from this study.

The evaluation procedure used here requires test fields for each training class be defined. Deleted classes are not specified by test fields and do not affect the classification accuracy for the classes being studied. In an operational system the entire frame is in effect a test field, and all classes present, whether or not they were included in the training classes, would effect the results. As stated above, the analysis of every class present in the total frame is beyond the scope of the present study. The classes studied here are barley, alfalfa, sugar beets, bare soil, and salt-affected bare soil called salt flats. These are the major crops and cover-types present in large quantity in this area. Water was also included in the classes studied. The statistical mean values for the film transmission data for the crop and soil classes studied here are presented in Figure 2 along with the classes discussed in the total frame analysis. These values represent uncalibrated spectral reflectances for these classes.

Sugar beets, alfalfa, and bare soil fields exhibited significant variations in their spectral responses and so the clustering facility was used to identify subclasses of these classes. The clustering algorithm defined seven subclasses of bare soil, two for sugar beets and two for alfalfa. Several statistically separate classes may exist for each class of agricultural importance. The classification process classifies statistically separate classes but computes performance by grouping together all subclass decisions for each agricultural class. For example, the clustering algorithm defined seven subclasses of bare soil. The classifier will classify on the basis of seven classes of soil, but results will be grouped into one class called bare soil.

The divergence analyzer was used to compute the pair-wise separability between the classes and subclasses studied. The divergence value is related to the squared distance between classes in a multidimensional pattern space. The pair-wise divergences are given in Table II for each of the 105 pairs of classes and subclass groups. These values serve to predict the degree of success that will be achieved by the classifier. The divergences between both barley subclasses and sugar beets subclass 3 are very small compared to other interclass divergences, which suggests that these subclasses are not very separable. Also sugar beets subclass 2 is nearly identical to alfalfa subclass 1, and sugar beets subclass 3 is similarly close to alfalfa subclass 2 indicating a lack of separability of these classes. Almost all of the other class pairs have relatively large divergences, and good separability is expected for these classes.

Samples of data from each of the classes defined by the clustering process were selected and used for training the pattern classifier. The major value of the histograms produced by LARSYSAA is to insure that the training sets chosen are approximately Gaussian. Test site 15A was represented by 66,000 data points and the training samples selected totaled 1132 or 1.7%. The data for test site 15D contained 27,300 points and 788 training samples (2.8%) were taken for this area. The statistics processor of the pattern classifier system was used to compute the training statistics for each of the classes selected. These statistics consist of the means and covariance matrices to be used by the Gaussian maximum likelihood classifier.

Two methods of statistical pattern recognition were used to classify the multiband imagery. One method classifies each image point into one of the defined classes. The other classifies an entire field as one decision. One advantage of the "per field" classification scheme, as it is called, is speed. A disadvantage is that the field coordinates must be determined and fed to the classifier before any classification can be performed. The per point classifier can classify any area without specified field boundaries, but it is a time-consuming process since every resolution element in an image is classified individually.

In order to evaluate the classification accuracy quantitatively, many test fields were extracted from the test sites. Of the total of 533 fields in the two flight lines, 174 were chosen as a test. Certain ones were deleted from the study because they were of a class not included in the training classes, or were too small to be defined in the imagery. The test fields are for the classes: barley, sugar beets, alfalfa, bare soil, salt flats, and water.

The per field classification was carried out for each of the fifteen possible combinations of the four channels available, as defined in Table II. A description of the fields and the classification results are presented in Tables IV and V. The maximum overall classification accuracy achieved for line 15A was 70.8% and for 15D was 70.6%. Study of the Dogwood Road results revealed that the accuracy for certain classes was relatively unrelated to the channels used. Bare soil and barley show relative constant classification accuracy for all cases where two or more channels are used. The accuracy for sugar beets recognition is best with all four channels and the alfalfa performance is poor in all cases. Salt flats and water were recognized with high accuracy in all cases. An interesting result was the high accuracy achieved by some of the classifications using only one or two channels. The highest accuracy for barley (82.1%) was achieved using only channel one (Panchromatic). The peak for bare soil, 100%, was obtained using channels 2 and 3 (green and infrared) and 3 and 4 (infrared and red). Equal maxima for several channel combinations were seen for alfalfa. The fields classified and the classification results are listed in Tables 4 and 5 for the four-channel classification.

The test sites were also classified using the per point classifier. The per point decision map for line 15A, Dogwood Road, is presented in Figure 5a, and the corresponding map for 15D, McCabe Road, is presented in Figure 6a with the classification symbols listed under the figures. Some of the roads in the areas are drawn in to aid in matching the results with the gray scale printout of the areas shown in Figure 4a and b. The test fields are indicated by a border of + signs. Figures 5b and 6b are test field border printouts to enable identification of the fields. The field numbers correspond to the ones in Table IV and V. The per point classification was not performed using all 15 of the possible combinations of the four available channels.

A comparison of the results of the per point and corresponding per field classification is presented in Table VI. The three channel (green, red, IR) and four channel (panchromatic, green, red, IR) comparisons are presented. The results are quite similar for the Dogwood Road site, but the per point sugar beet and salt flat classification was poor compared to the per field results for the McCabe Road test. This indicates that the training data for the McCabe Road area were not as complete as for the Dogwood Road area. The per field classifier is evidently able to give better results using incomplete training data. This result also tends to indicate the value of clustering as a method of training analysis. Although clustering was used for both the Dogwood and McCabe areas, the individual cluster points were used as training for the Dogwood area only. For the McCabe Road area the clustering results were used to select the entire field as training, and there was most likely more than one subclass in the field. The resulting mixture of classes can cause the per point results to be poorer than the per field results in that a field having a majority of points in a particular class will most likely be classified into that class by the per field classifier. The per point classifier will count all the points not classified into the class assigned to the field as errors. For example, if 75% of the points in a barley field looked like barley and 25% looked like alfalfa, the per field classifier would probably call the entire field barely and claim a 100% accuracy. The per point classifier would list the accuracy on the field as 75%.

The analysis discussed up to this point used data from the multiband black and white exposures only. Color separations data from the color infrared film was obtained by scanning the film with blue, green, and red filters in turn to separate the densities of the three dyes. The digitized density data from the three scans were then registered and analyzed in the same manner as the multispectral black and white film data. The Dogwood Road test site data were classified using the per field classifier and the same training and test areas used for the multispectral B & W analysis. The comparative results are listed in Table VII using the results for the per field multiband black and white classification as reference. The overall difference is only -2.3%. The differences for the two major crops, however were quite significant, barley decreasing by 16.7% and sugar beets improving by 10.8%. This evidence is insufficient to conclude that one film sensor is superior to the other; however, this result agrees with the intuitive expectation that the multilayer color film structure somewhat degrades the spectral resolution compared to that obtainable using separate film-filter sensors.

The general conclusion indicated by the classification results is that specific breakdowns of crop types is difficult from three band satellite photography and in some cases impossible. The results were obtained, however, from uncalibrated photography having considerable overlap of the spectral bands, and other distortions in the spectral data were present. Improved photographic fidelity with more and better-separated spectral bands may result in significantly better crop separation accuracies.

Figures 5 and 6 offer a qualitative evaluation of the classifier performance. Inspection of these printouts reveals that the basic structure of the field patterns, roads, cities, etc., is captured by the classifier. One can extrapolate the successful classifications shown by the bordered test fields to other parts of the area to obtain a judgement of the overall performance. The area classified in lines 15A and 15D was approximately 135 square miles represented by 93,900 resolution elements. The test fields included 5906 of these points which covered 12,474 acres. Although the performance of the classifier appears to be good over a large area, the usefulness of the automatic processing approach will depend on the accuracy requirements of the particular application.

7. SOIL MAPPING EXPERIMENTS

Soil scientists at LARS attempted to use the digitized Apollo 9 data to identify the soil patterns or soil associations in the area of El Centro in the Imperial Valley, California. The El Centro area in Imperial County is located in the Southeast portion of California. It covers 540 acres and has quite uniform topography which is slightly rolling and in some places broken by sand dunes. The climate is dry and irrigation is necessary for the growth of cultivated crops. The soils of the study area are generally young and the surface soils and subsoils are very much alike. The material which forms the soils consists primarily of sediment deposited by the Colorado River, and local alluvium from the California coastal range of the Chocolate Mountains. A new soil map of the area of the Imperial County was not available so the study used representative soil groups which were found in a soil map published in 1918, Figure 7, and in a description found in a Soil Survey of the El Centro area, California, 1922. Also, a report for the general soil map for the Imperial County, California, 1967 was used. Two sand types, four loamy and one clayey soil were found to be spectrally separable in the study.

These were: Rositas fine sand and Rositas very fine sand consisting of light yellowish brown incoherent sand developed in the eastern and western parts of the area associated with the very fine sand and with sand dunes. Larger areas of Rositas fine sand are located between the Alamo River and the Ash Canal (see Figure 7). Southeast of El Centro, west of Holtville, smaller bodies of Rositas fine sand exist.

Rositas fine sand and Rositas very fine sand consist of 80-90% incoherent sands, 5-7% silt, 2-7% clay and very low amounts of organic matter. They are very well drained. The surface of both sands are light yellowish brown or yellowish gray. Since the Rositas very fine sand contains higher percentages of very fine sands, the surface is much more compact. Both sands have high reflectance in all portions of the spectrum (see Table VIII). On the basis of their physical characteristics, the pattern recognition system had no problem in detecting and separating sand-covered surfaces from other bare soils in the investigated area.

South of Holtville and east of El Centro are areas with very fine sand of the Rositas series mixed with 10-35% silt and 10-12% clay known as Meloland fine sandy loam. Since the amount of sand is 30-70%, and the silt, clay and organic matter is increased, the color of these soils is darker than the Rositas sands. The spectral reflectance values are much lower throughout the spectral wavelength bands.

Since the difference in physical and chemical properties of the soil cause differences in soil spectral responses, we expected to detect spectrally other soils with higher content of silt and clay than just the Meloland fine sandy loam. South of the Meloland, in the vicinity of Bowker Road are oases of Holtville soils containing about 50% silt, 25% clay, and 1-40% fine sand and very fine Rosita sands. These soils are developed on nearly level flood plains and old lake bottoms. The surface layers are light brown silty clay loam. Table VIII shows values of reflected spectral energy of Holtville loams of two locations in the El Centro

area. Both Holtville soils have very close relative reflectance values in all parts of the spectrum. They both absorb much more of incident solar energy than sands and sandy soils.

Imperial Soils located between Ash Canal and Anderholt Road and scattered south of Holtville and Meloland are lighter in color than Holtville soils having lower silt content. They occur on nearly level bottoms of old lake beds. They are highly calcareous and usually contain gypsum and soluble salts. The amount of reflected solar energy of Imperial loams is higher than that of Holtville soils. Imperial soils with 35% clay and high organic content and with poor natural drainage - called Imperial silty clays - reflect much less than the loamy and sandy soils.

Training samples of these soil types were selected and used to train the pattern classifier. The classification map produced for the area shown in the abstracted soil map in Figure 7 is presented in Figure 8. The various classification decisions are shown as shades of gray and annotated by arrows. The computer classification map differs greatly from the soil map due to the fields of green vegetation covering most of the area which block the soil background. Also, cultural influences occurring over a period since the date of the map (1918) have changed the apparent soil structure of the area.

Many bare soil "fields" were correctly classified, however, and the high reflectance sand areas were readily recognized. Quantitative evaluation of the classifier performance was not determined in the study reported here. Instead, study of the spectral characteristics of areas of known soil type was emphasized. Separability of the soil types in this area was established using the three-band film data. The conclusion of this part of the study is that the three-band spectral data gathered at satellite altitude shows great promise for large-scale soil mapping.

8. GEOLOGICAL MAPPING EXPERIMENTS

Basically, geological mapping is a method of expressing, at a manageable scale, the spatial distribution of rock types. Previous photointerpretation studies of the satellite photographs of this area did not achieve the required differentiation between materials of geological interest to provide the geologist with an adequate tool for differentiating rock types. The main purpose of this study was to determine what rock units could be distinguished in the Apollo 9 photography using multiband pattern recognition techniques.

The only "ground truth" used for the study was the San Diego-El Centro and Salton Sea sheets of the California Geological Map. In addition, a more detailed preliminary manuscript map of the area was provided by Mr. P. K. Morton of the California Division of Mines and Geology. Figure 9 is a generalized map based on the above mentioned maps. Within the study area the rock units were divided into the major groupings listed in Table IX.

Detailed analysis of the Cargo Muchacho-Chocolate Mountains area was performed to determine if the bedrock material could be differentiated. In these analyses the computer was trained with samples taken from fields representing every major rock type as well as other features such as water, etc.

The results of this detailed analysis are shown in Figure 10. The overall correlation between the computer-classification maps and the generalized geological map (Figure 9) is excellent, with many of the most prominent geological features well-mapped and distinguishable. The major rock groups can not only be differentiated, but they can also be identified. Such features as contacts (marked 1 and 2 respectively in Figure 10) and faults (marked 3 and 4) can be readily recognized.

It was found that several spectral classes were necessary in order to map adequately a single rock type. For example, as many as ten spectral classes could be assigned to granite. Examination of these spectral classes with reference to the topographic features portrayed in the geologic maps, indicated not only that the overall tone of the rock types was important but also that topography played a major role in the spectral response of the various rock units. The number of spectral classes which were significant in each major rock type and the maximum relief for the rock types are summarized in Table X.

It was noted that ridges and highs tend to display the least reflectance within any given rock unit and that reflectance tends to increase down the slopes with the low, flat areas displaying the highest reflectance. Area (5), Figure 10 in the northern Cargo Muchacho Mountains is an area mapped as granite. The computer display shows the granite pattern best as a series of linear elements which correspond to the ridges in the area.

The results of the geological study were encouraging. The three spectral bands of the Apollo 9 photographs were sufficient for differentiating the major rock units in this particular area. It was found that even though relief presents a problem, the overall distribution of rock types can be determined. The map constructed from the spectral classification simulated the geologic map quite well, and it appears that large scale, automatic reconnaissance geologic mapping can be performed using multiband photography.

9. SUMMARY AND CONCLUSIONS

The results of this experiment of reducing uncalibrated space photography to useful information are promising. Many earth surface features were distinguishable using multispectral measurements collected from a satellite platform. The data handling techniques required for the conversion of photographic measurements to a multispectral data base require further study. The initial results obtained in this experiment coupled with other current research findings encourage the use of multiband photography as a multispectral data collection instrument. More important is the promise shown for automatic reduction of multispectral measurements from satellite platforms to useful management information.

The data registration technique used in this experiment to overlay the multispectral black and white photographs continues to be researched. At present the techniques require a large computational resource for each area of interest. Future capabilities such as optical processing techniques or an improved algorithm may greatly reduce this cost of data handling as well as increase the number of measurement dimensions (i.e., make more temporal measurements available). A second method of decreasing registration costs is the use of multiemulsion (i.e., color) photography. Improvements in the properties of each layer of this type of film are required to enable measurements of narrower bands of energy. Increased ability to convert these measurements to calibrated electronic signals is also required. This will solve the registration problem and also enhance the information content of the photograph. The results of using trilayer film in this experiment encourage further development toward these goals. The third method of decreasing the data handling requirements is the use of multispectral scanners at satellite altitude. This, coupled with the classification results reported here enhances the expectations of future remote sensing systems. The concept of storing image measurements on film and retrieving them for later use should continue to be researched.

<u>Code</u>	<u>Film</u>	<u>Filter</u>	<u>Band</u>
A	SO-180 Ektachrome Infrared	Photar 15	.51-.89 micrometers
B	3400 Panatomic-X	Photar 58B	.47-.61 micrometers
C	SO-246 B/W Infrared	Photar 89B	.68-.89 micrometers
D	3400 Panatomic-X	Photar 25A	.59-.715 micrometers

TABLE I. FILM FILTER COMBINATIONS USED IN SO-65 EXPERIMENT

Four Hasselblad cameras with 80 mm focal lengths were
used for space use

Channel Number	Wavelength Band (Micrometers)	Band Description
1	.51 - .89	Panchromatic
2	.47 - .61	Green
3	.59 - .71	Red
4	.68 - .89	Infrared

TABLE II. WAVELENGTH BANDS AND DATA SETS USED IN ANALYSIS

TABLE III. INTERCLASS DIVERGENCE MATRIX

(Area 15A (Dogwood Road)
Channels 2,3,4

		Barley		Sugar Beets			Alfalfa		Bare Soil						Wa- ter	
Subclass		1	2	1	2	3	1	2	1	2	3	4	5	6		
Barley	1		8	204	96	13	98	32	566	354	589	436	511	488	1521	712
	2			89	36	2	35	8	281	162	313	222	269	318	879	431
Sugar Beets	1				24	75	22	63	74	26	94	37	94	71	518	285
	2					24	3	15	194	91	223	126	200	164	829	412
	3						29	4	280	168	306	206	254	264	933	431
Alfalfa	1							21	180	78	192	110	181	169	784	378
	2								273	149	293	182	245	245	960	496
	1									25	28	28	75	92	201	291
	2										54	27	101	120	337	307
	3											18	19	75	265	196
	4												24	32	346	219
	5													28	268	135
	6														404	218
Salt Flat																264

TABLE IV. PER FIELD CLASSIFICATION

Test fields in the Dogwood Road area (flightline 15A);
data collected in the .51-.79, .46-.61, .68-.89, .59-.71
micrometer ranges.

<u>Field No.</u>	<u>Ground Truth Classification</u>	<u>% Ground Cover</u>	<u>Acres</u>	<u>Computer Classification</u>
2	Barley	95	76	Barley
6	Barley	96	116	Barley
12	Barley	95	85	Barley
17	Barley	100	53	Sugar Beets
18	Barley	100	66	Barley
19	Barley	100	70	Barley
20	Barley	90	55	Alfalfa
36	Barley	100	110	Barley
47	Barley	100	104	Barley
48	Barley	100	36	Barley
71	Barley	100	77	Barley
76	Barley	80	15	Barley
104	Barley	90	113	Barley
105	Barley	95	57	Sugar Beets
119	Barley	60	138	Sugar Beets
143	Barley	40	12	Bare Soil
173	Barley	100	24	Barley
198	Barley	100	36	Barley
199	Barley	100	32	Barley
213	Barley	95	139	Barley
227	Barley	90	42	Barley
240	Barley	90	32	Sugar Beets
243	Barley	100	72	Barley
244	Barley	100	80	Barley
249	Barley	95	95	Barley
279	Barley	100	58	Barley
284	Barley	80	104	Barley
285	Barley	100	24	Barley
Total Barley Acreage			1921	

TABLE IV. CONTINUED

<u>Field No.</u>	<u>Ground Truth Classification</u>	<u>% Ground Cover</u>	<u>Acres</u>	<u>Computer Classification</u>
16	Sugar Beets	90	28	Alfalfa
51	Sugar Beets	95	215	Sugar Beets
52	Sugar Beets	90	67	Sugar Beets
55	Sugar Beets	75	148	Alfalfa
59	Sugar Beets	95	70	Alfalfa
62	Sugar Beets	80	136	Sugar Beets
66	Sugar Beets	80	77	Sugar Beets
77	Sugar Beets	90	65	Sugar Beets
154	Sugar Beets	90	162	Sugar Beets
163	Sugar Beets	90	10	Sugar Beets
164	Sugar Beets	90	18	Sugar Beets
245	Sugar Beets	95	36	Barley
248	Sugar Beets	80	66	Sugar Beets
268	Sugar Beets	90	97	Sugar Beets
262	Sugar Beets	80	62	Sugar Beets
266	Sugar Beets	95	74	Barley
267	Sugar Beets	90	36	Sugar Beets
289	Sugar Beets	60	83	Sugar Beets
290	Sugar Beets	60	148	Sugar Beets
291	Sugar Beets	70	92	Alfalfa
292	Sugar Beets	70	92	Sugar Beets
298	Sugar Beets	40	80	Barley
		Total Sugar Beet Acreage	1867	
13	Alfalfa	95	85	Sugar Beets
15	Alfalfa	100	21	Barley
14	Alfalfa	100	73	Barley
22	Alfalfa	90	94	Alfalfa
42	Alfalfa	70	165	Sugar Beets
39	Alfalfa	85	140	Sugar Beets
50	Alfalfa	80	24	Sugar Beets
58	Alfalfa	95	120	Sugar Beets
186	Alfalfa	60	32	Sugar Beets
282	Alfalfa	80	42	Sugar Beets
288	Alfalfa	95	67	Barley
		Total Alfalfa Acreage	863	

TABLE IV. CONTINUED

<u>Field No.</u>	<u>Ground Truth Classification</u>	<u>% Ground Cover</u>	<u>Acres</u>	<u>Computer Classification</u>
1	Bare Soil			Bare Soil
5	Bare Soil		94	Bare Soil
7	Bare Soil		106	Bare Soil
8	Bare Soil		94	Bare Soil
11	Bare Soil		85	Bare Soil
21	Bare Soil		42	Bare Soil
44	Bare Soil		35	Bare Soil
41	Bare Soil		94	Bare Soil
45	Bare Soil		67	Bare Soil
46	Bare Soil		91	Bare Soil
61	Bare Soil		115	Bare Soil
155	Bare Soil		35	Bare Soil
157	Bare Soil		93	Salt Flat
222	Bare Soil		77	Bare Soil
230	Bare Soil		36	Salt Flat
258	Bare Soil		28	Bare Soil
269	Bare Soil		83	Sugar Beets
		Total Bare Soil Acreage	1175	
98	Salt Flat		260	Salt Flat
101	Salt Flat		190	Salt Flat
106	Salt Flat		114	Salt Flat
125	Salt Flat		75	Salt Flat
126	Salt Flat		37	Salt Flat
127	Salt Flat		43	Salt Flat
128	Salt Flat		77	Salt Flat
158	Salt Flat		54	Salt Flat
159	Salt Flat		9	Salt Flat
221	Salt Flat		129	Salt Flat
		Total Salt Flat Acreage	988	
99	Water		350	Water
		Overall Total	7164	

TABLE V. PER FIELD CLASSIFICATION

Test fields in the McCabe Road area (flightline 15D);
 data collected in the .51-.79, .46-.61, .68-.89, .59-.71
 micrometer ranges.
 (Acreages not available)

<u>Field No.</u>	<u>Ground Truth Classification</u>	<u>% Ground Cover</u>	<u>Computer Classification</u>
235	Barley	90	Sugar Beets
101	Barley	100	Barley
100	Barley	100	Barley
130	Barley	100	Barley
2	Barley	60	Sugar Beets
116	Barley	80	Sugar Beets
213	Barley	90	Barley
202	Barley	100	Barley
75	Barley	95	Barley
26	Barley	90	Sugar Beets
115	Barley	90	Sugar Beets
19	Barley	80	Barley
48	Barley	90	Sugar Beets
62	Barley	90	Sugar Beets
18	Barley	100	Barley
90	Barley	90	Barley
198	Barley	100	Barley
79	Barley	100	Barley
60	Barley	100	Barley
89	Barley	100	Barley
80	Barley	100	Barley
52	Barley	100	Barley
34	Barley	90	Barley
82	Barley	80	Barley
16	Barley	90	Barley
59	Barley	70	Barley
87	Barley	70	Barley
83	Barley	90	Alfalfa
15	Barley	90	Barley
58	Barley	70	Alfalfa
57	Barley	100	Barley

TABLE V. CONTINUED

<u>Field No.</u>	<u>Ground Truth Classification</u>	<u>% Ground Cover</u>	<u>Computer Classification</u>
179	Sugar Beets	90	Alfalfa
40	Sugar Beets	80	Sugar Beets
190	Sugar Beets	100	Sugar Beets
178	Sugar Beets	90	Alfalfa
214	Sugar Beets	70	Sugar Beets
39	Sugar Beets	90	Sugar Beets
74	Sugar Beets	90	Sugar Beets
63	Sugar Beets	90	Sugar Beets
170	Sugar Beets	80	Barley
86	Sugar Beets	90	Sugar Beets
55	Sugar Beets	100	Sugar Beets
160	Alfalfa	90	Alfalfa
159	Alfalfa	95	Alfalfa
185	Alfalfa	90	Alfalfa
225	Alfalfa	100	Sugar Beets
124	Alfalfa	100	Sugar Beets
99	Alfalfa	100	Barley
236	Alfalfa	100	Barley
119	Alfalfa	90	Alfalfa
223	Alfalfa	90	Sugar Beets
104	Alfalfa	80	Alfalfa
117	Alfalfa	80	Barley
177	Alfalfa	100	Barley
216	Alfalfa	100	Alfalfa
29	Alfalfa	90	Barley
17	Alfalfa	100	Sugar Beets
51	Alfalfa	90	Barley
171	Alfalfa	100	Barley
14	Alfalfa	90	Alfalfa
12	Alfalfa	90	Alfalfa
209	Bare Soil		Bare Soil
158	Bare Soil		Bare Soil
127	Bare Soil		Bare Soil
157	Bare Soil		Bare Soil
128	Bare Soil		Bare Soil

TABLE V. CONTINUED

<u>Field No.</u>	<u>Ground Truth Classification</u>	<u>% Ground Cover</u>	<u>Computer Classification</u>
156	Bare Soil		Bare Soil
163	Bare Soil		Bare Soil
122	Bare Soil		Bare Soil
103	Bare Soil		Bare Soil
164	Bare Soil		Bare Soil
118	Bare Soil		Bare Soil
45	Bare Soil		Bare Soil
135	Bare Soil		Bare Soil
201	Bare Soil		Bare Soil
166	Bare Soil		Bare Soil
168	Bare Soil		Bare Soil
76	Bare Soil		Bare Soil
151	Bare Soil		Bare Soil
169	Bare Soil		Bare Soil
114	Bare Soil		Bare Soil
77	Bare Soil		Salt Flat
73	Bare Soil		Bare Soil
61	Bare Soil		Salt Flat
47	Salt Flat		Salt Flat

TABLE VIa. COMPARISON OF PER FIELD AND PER POINT
RESULTS USING CHANNELS 1,2,3,4

Class	Dogwood Road				McCabe Road			
	<u>Fields</u>	<u>Per Field</u>	<u>Sams</u>	<u>Per Point</u>	<u>Fields</u>	<u>Per Field</u>	<u>Sams</u>	<u>Per Point</u>
Barley	28	78.6%	911	72.7%	31	67.7%	832	70.8%
Sugar Beets	22	68.2	1046	43.6	11	54.5	406	27.8
Alfalfa	11	9.1	395	36.0	19	42.1	564	41.7
Bare Soil	10	82.4	615	77.6	23	95.7	695	86.3
Salt Flats	17	100.0	359	59.9	1	100.0	21	4.8
Water	1	100.0	72	97.2	0	-----	0	-----
OVERALL		70.8%		60.0%		68.2%		61.1%

TABLE VIb. COMPARISON OF PER FIELD AND PER POINT
RESULTS USING CHANNELS 2,3,4

Class	Dogwood Road				McCabe Road			
	<u>Fields</u>	<u>Per Field</u>	<u>Sams</u>	<u>Per Point</u>	<u>Fields</u>	<u>Per Field</u>	<u>Sams</u>	<u>Per Point'</u>
Barley	28	75.0%	911	71.2%	31	71.0%	832	76.6%
Sugar Beets	22	59.1	1046	48.5	11	72.7	406	26.6
Alfalfa	11	27.3	395	38.2	19	42.1	464	39.2
Bare Soil	17	82.4	615	77.2	23	91.3	695	85.8
Salt Flats	10	100.0	359	70.5	1	100.0	21	9.5
Water	1	100.0	72	98.6	0	-----	0	-----
OVERALL		69.7%		62.0%		70.6%		62.1%

TABLE VII. COMPARISON OF MULTIBAND AND MULTIBASE RESULTS
FOR DOGWOOD ROAD (LINE 15A). (Per Field Results)

B & W FILTERED FILM DATA		COLOR SEPARATION OF COLOR INFRARED FILM DATA	DIFFERENCE
Barley	70.6%	53.9%	-16.7%
Alfalfa	40.0	35.8	- 4.2
Sugar Beets	31.9	42.7	+10.8
Bare Soil	62.1	57.6	- 4.5
Salt Flat	88.4	92.8	+ 4.4
Water	99.1	95.5	- 3.6
OVERALL	59.3%	57.0%	- 2.3%

TABLE VIII. RELATIVE SPECTRAL REFLECTANCE IN DIFFERENT
WAVELENGTH BANDS (MICROMETERS)

	<u>0.47-0.89</u>	<u>0.47-0.61</u>	<u>0.68-0.89</u>	<u>0.59-0.71</u>
Fine sand	339.78	120.55	110.86	108.37
Very fine sand	324.21	116.97	103.92	103.32
Meloland fine sandy loam	286.17	103.84	98.92	83.41
Imperial Silty Clay Loam	284.64	104.20	97.39	83.05
Holtville Silty Clay Loam Type 1	286.81	94.53	91.47	82.81
Holtville Silty Clay Loam Type 2	263.97	95.65	85.72	82.60
Imperial Silty Clay	250.19	91.84	80.87	77.48

TABLE IX. DESCRIPTION OF MAJOR ROCK UNITS

Sand dunes. Unconsolidated.

Sand and Silty Sand. (Includes both Recent and Pleistocene age material).

Undifferentiated Slope Material Including Alluvium. Unconsolidated clay, silt, sand and gravel occurring primarily as valley fill and streamwash deposits.

Older Alluvium. Partly dissected, largely unconsolidated, poorly sorted silt, sand, and gravel of alluvial fans, margins of larger canyons, and terraces.

Quaternary-Cenozoic Volcanics. Basalt flows, fine grained vesicular basalt and minor interbedded conglomerates.

Tertiary Volcanics Undifferentiated. Andesitic and rhyolitic intrusives and pyroclastics. Includes several separable units and ages.

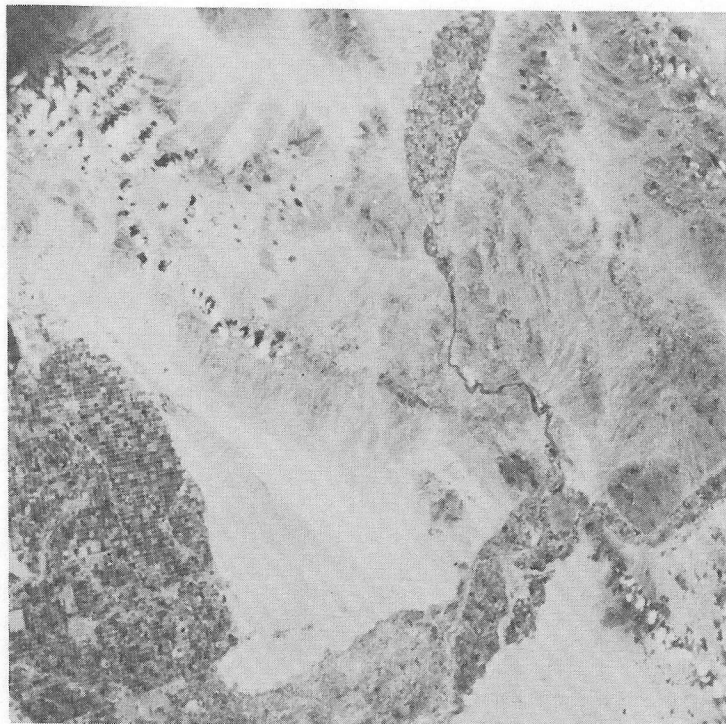
Mesozoic Granites. Biotite granite, leucogranite, quartz diorite, and quartz monzonite.

Pre-Tertiary Metasediments and Metavolcanics. Paleozoic to Mesozoic in age. Predominantly biotite schist quartzites, gneisses and marbles.

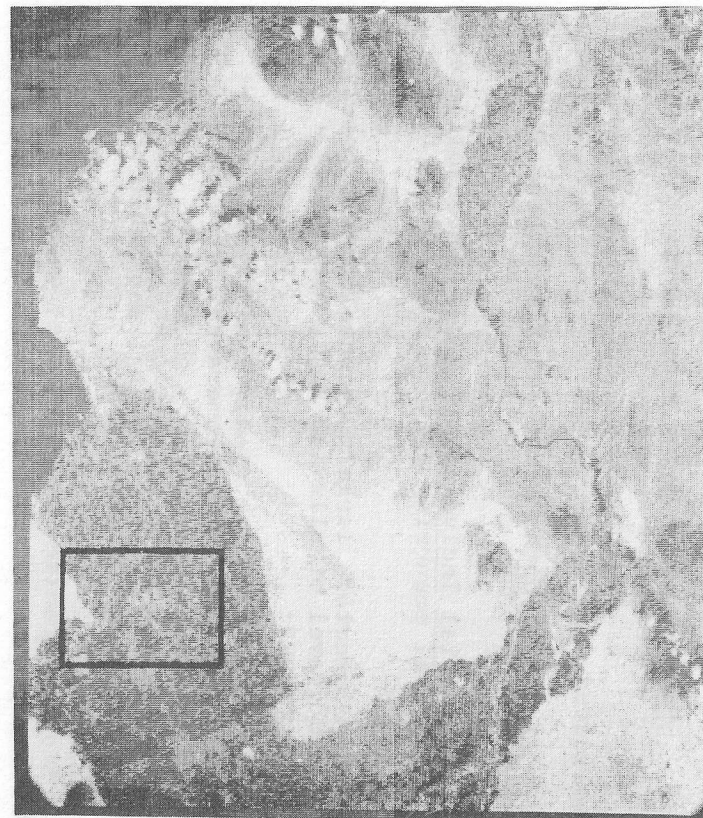
Precambrian Basal Complex. Undifferentiated metamorphic and igneous rocks.

TABLE X. NUMBER OF SPECTRAL CLASSES VERSUS TOPOGRAPHIC RELIEF

<u>Rock Type</u>	<u>Maximum Topo- graphic Relief in Feet</u>	<u>Number of Spectral Classes</u>
Sand	200	1
Alluvium	400	3
Quaternary Cenozoic Volcanics	1000	7
Tertiary Volcanics	1100	8
Mesozoic Granite	1800	10
Pre-Tertiary Metamorphic	700	5
Precambrian Basal Complex	600	3



1a Apollo 9 Photograph
(black and white rendition)



1b Computer Generated Image

Figure 1. Photographic Print of Apollo 9 Frame 3698 and Computer Generated Image of the Digitized Frame

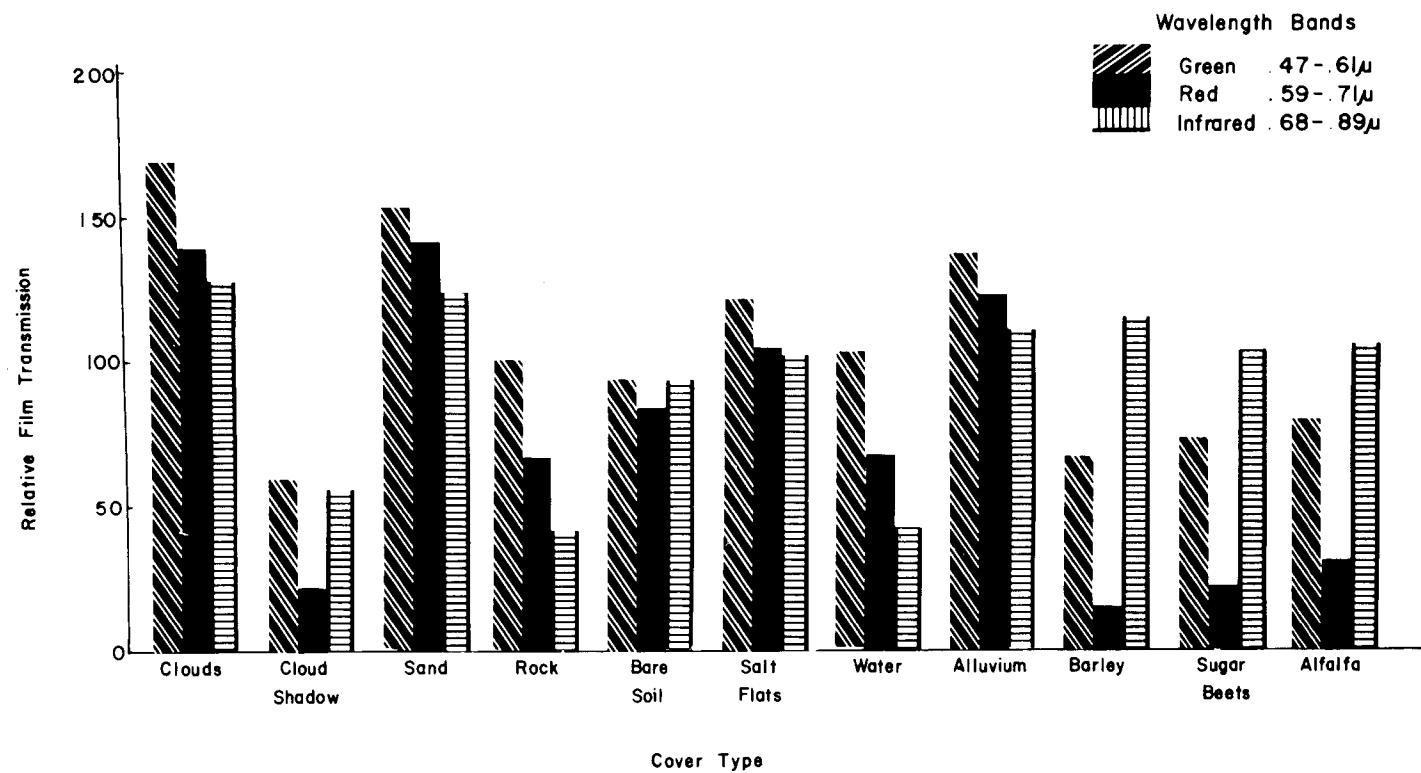


Figure 2. Relative Spectral Reflectance for Cover Types Studied

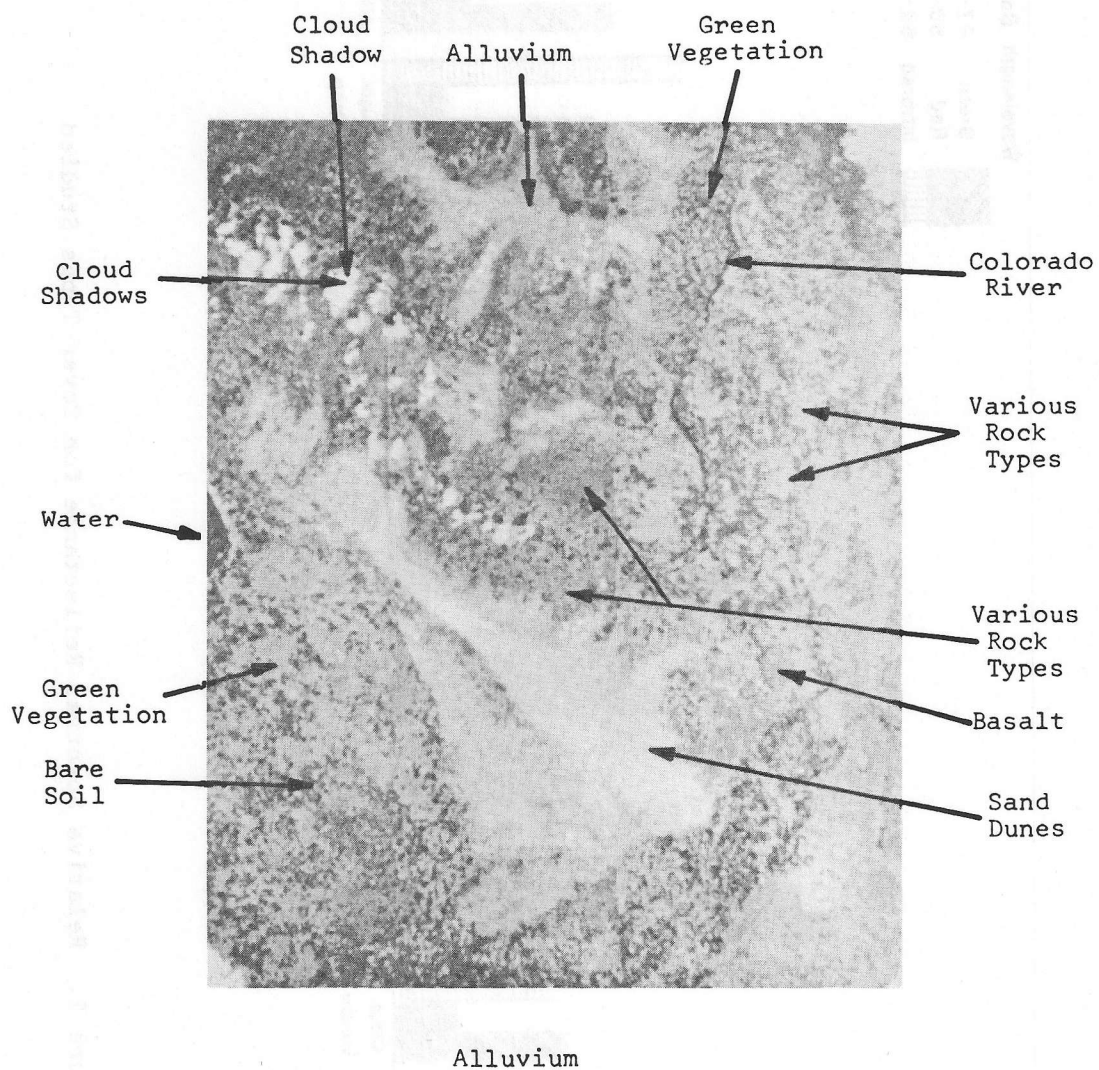


Figure 3. Synoptic Computer Classification Map of Apollo 9 Frame 3698. Gray Tone Encoded.

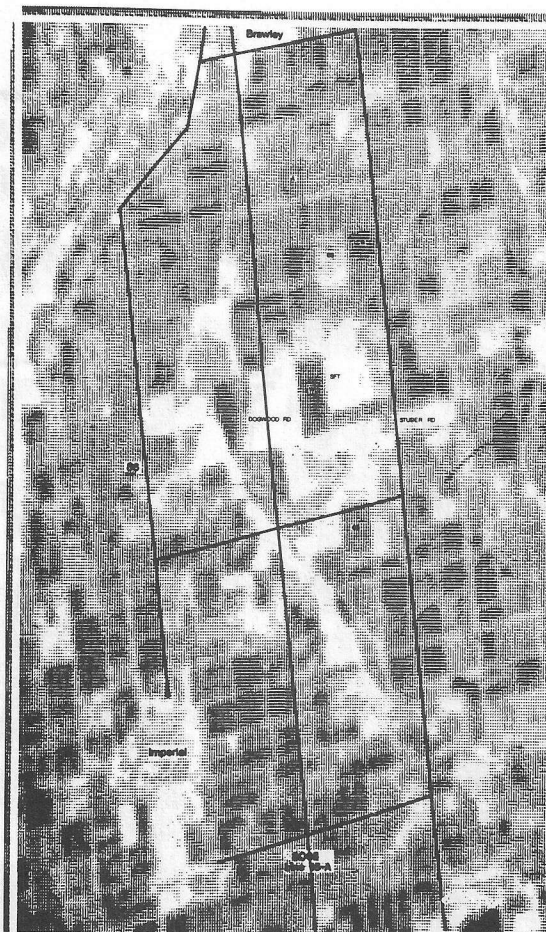
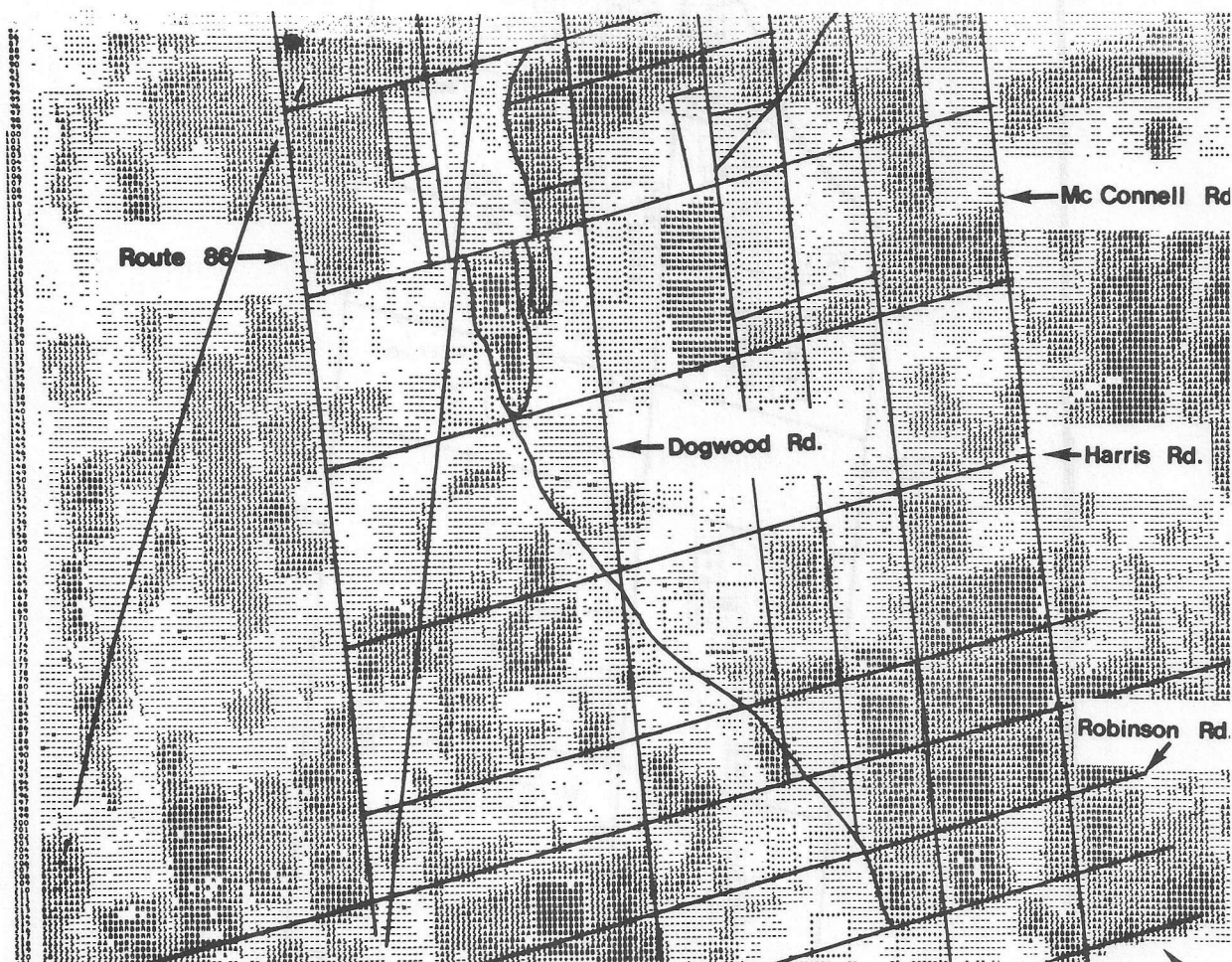


Figure 4a. Gray Scale Printout of Dogwood Road Area (S065 Site 15A)



Figure 4b. Gray Scale Printout of McCabe Road Area (S065 Site 15D)

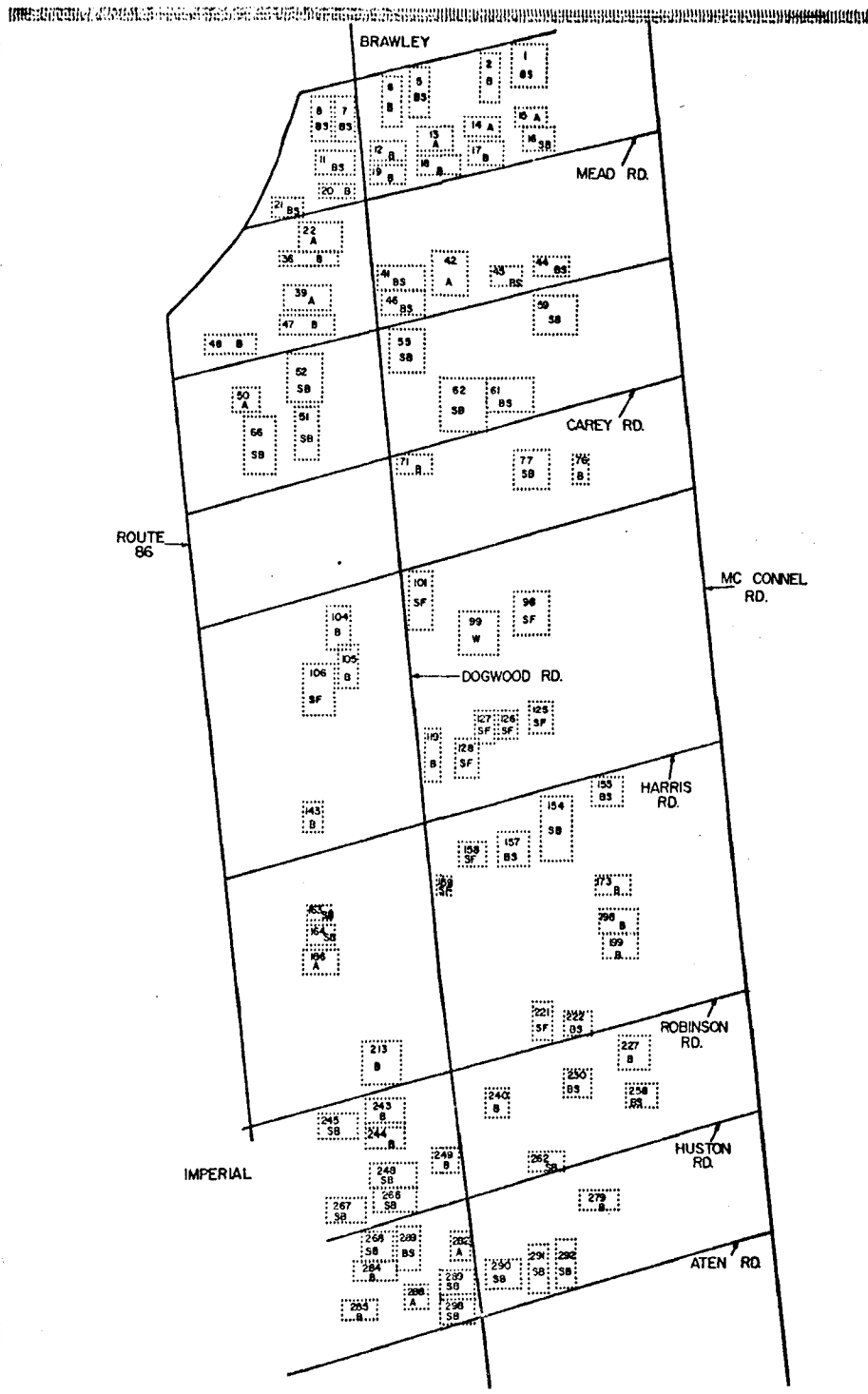


SYMBOL KEY

B Barley
A Alfalfa
S Sugar Beets

• Salt Flat
- Bare Soil
W Water

Figure 5a. Per Point Classification Printout for Area 15A (Dogwood Road). Test fields outlined with + signs.



SYMBOL KEY

B Barley
SB Sugar Beets
A Alfalfa

BS Bare Soil
SF Salt Flats
W Water

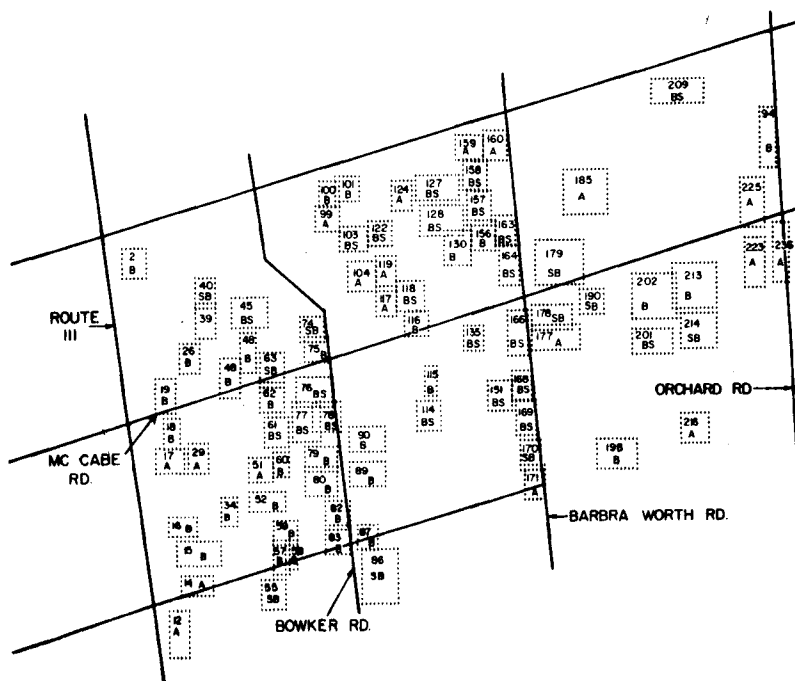
Figure 5b. Test Field Border Map For Dogwood Road Area
Test Site



SYMBOL KEY

B Barley	- Bare Soil
S Sugar Beets	I Salt Flats
A Alfalfa	

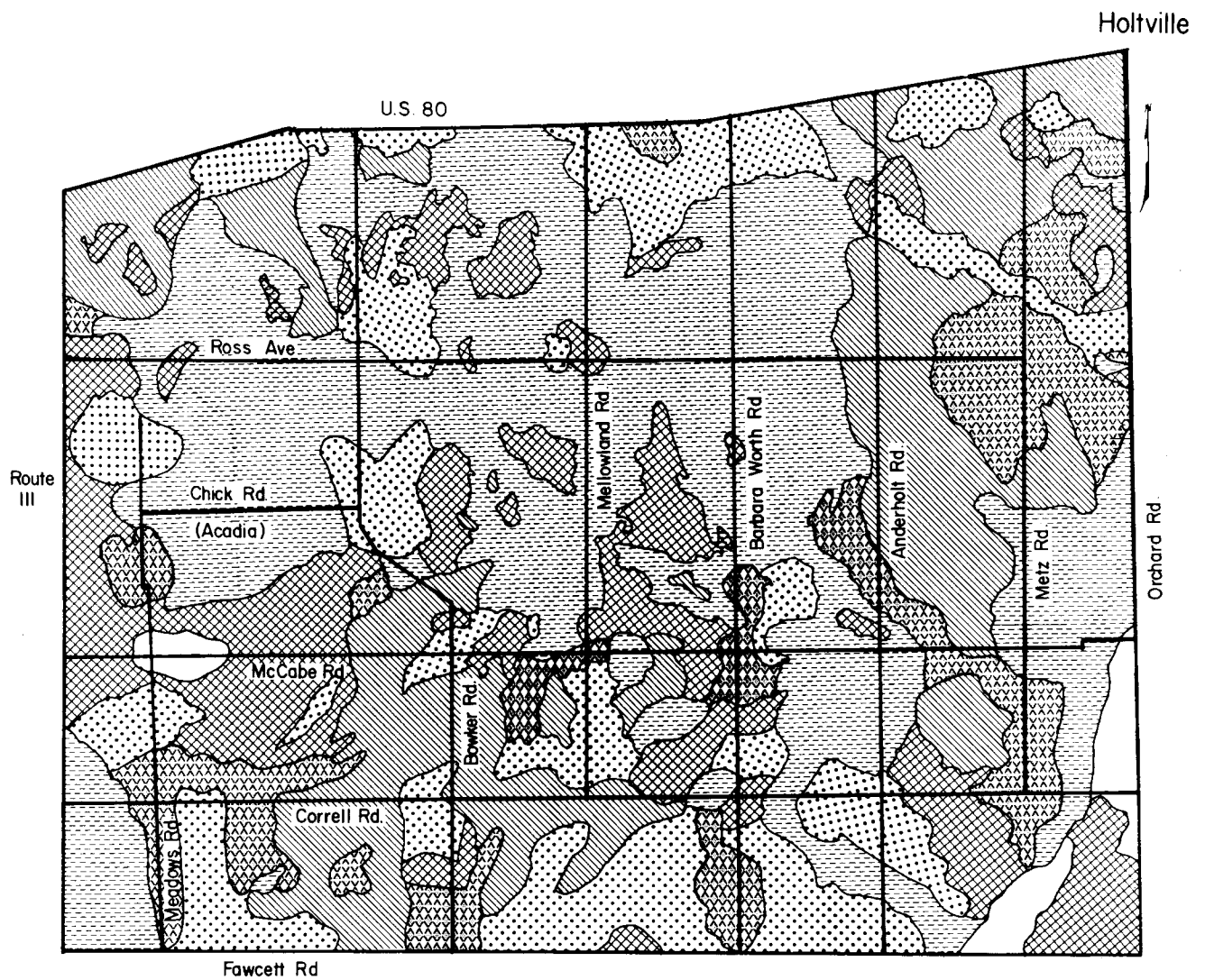
Figure 6a. Per Point Classification Printout for Area 15D (McCabe Road). Test fields outlined with + signs.



SYMBOL KEY

B Barley	BS Bare Soil
SB Sugar Beets	SF Salt Flats
A Alfalfa	

Figure 6b. Test Field Border Map for McCabe Road Test Site



SYMBOL KEY




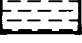

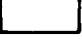
	Imperial Silty Clay		Rositas & Dune Sand
	Holtville Silty Clay & Loam		Meloland Fine Sandy Loam
	Imperial Silty Clay Loam		Holtville Very Fine Sandy Loam

Figure 7. Generalized Soil Map of El Centro, California Area.

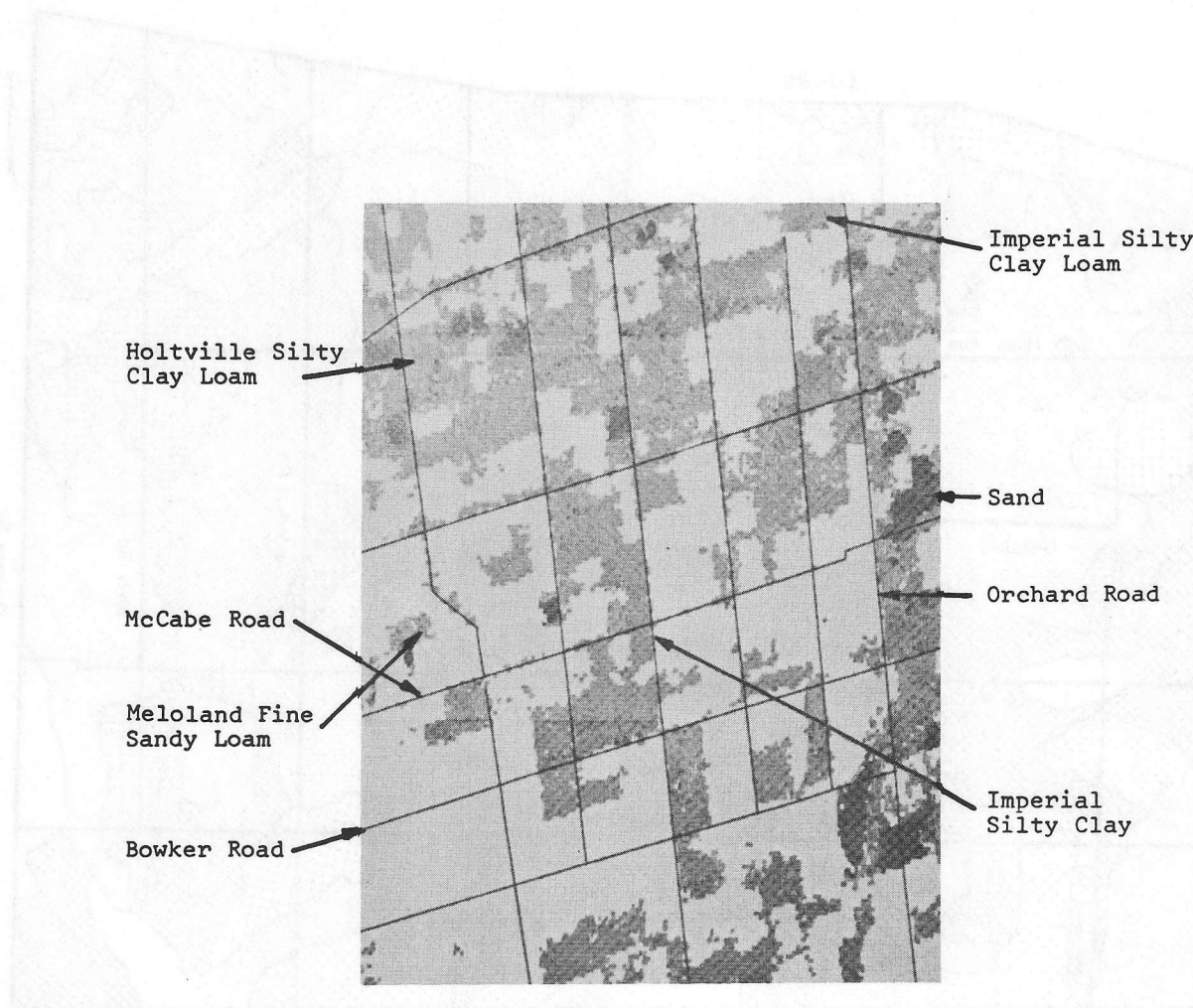


Figure 8. Computer Classification Map of Soils
in the El Centro, California Area.
(black and white rendition)

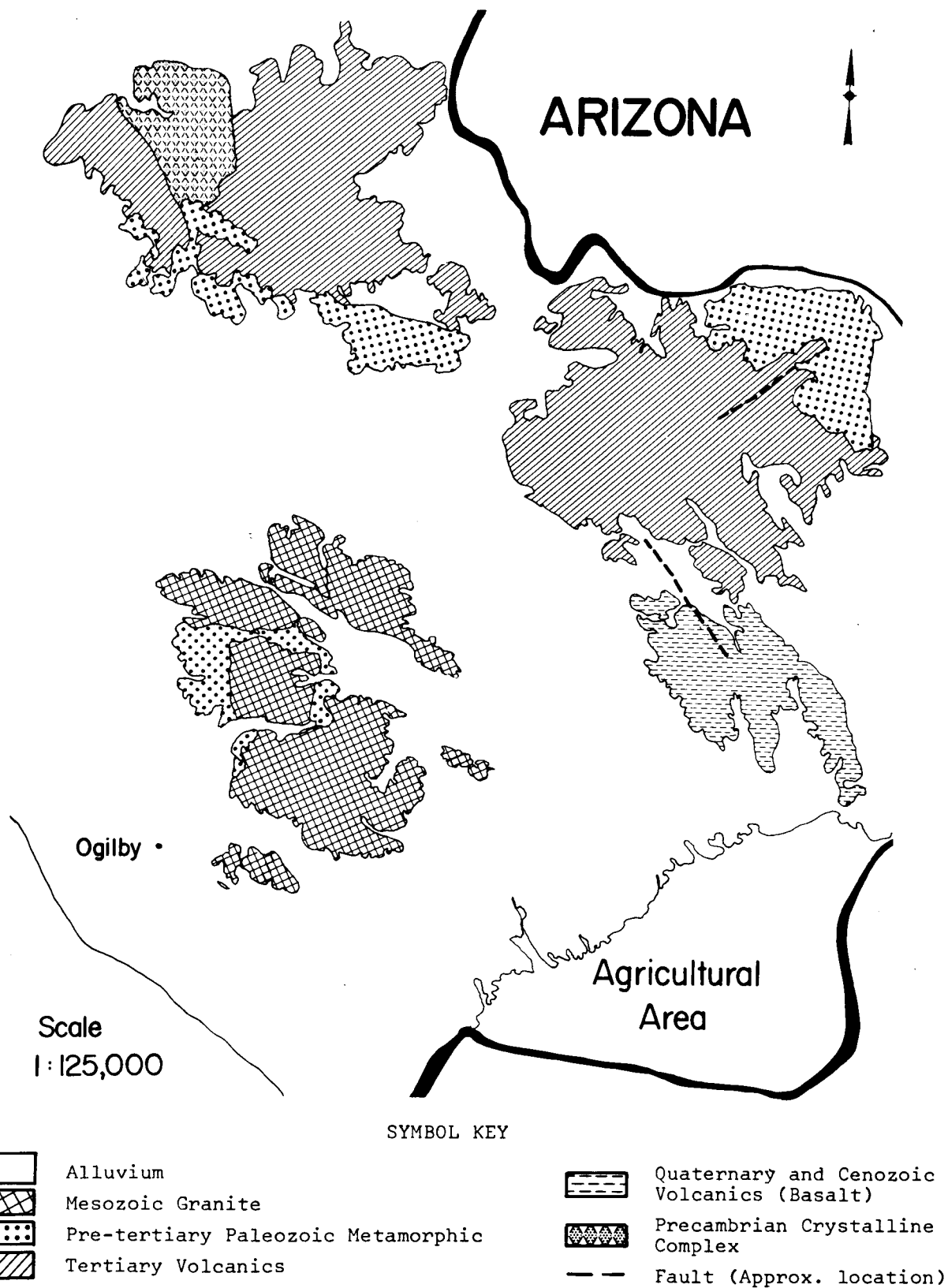


Figure 9. Generalized Geological Map of Chocolate Mountain Area, California

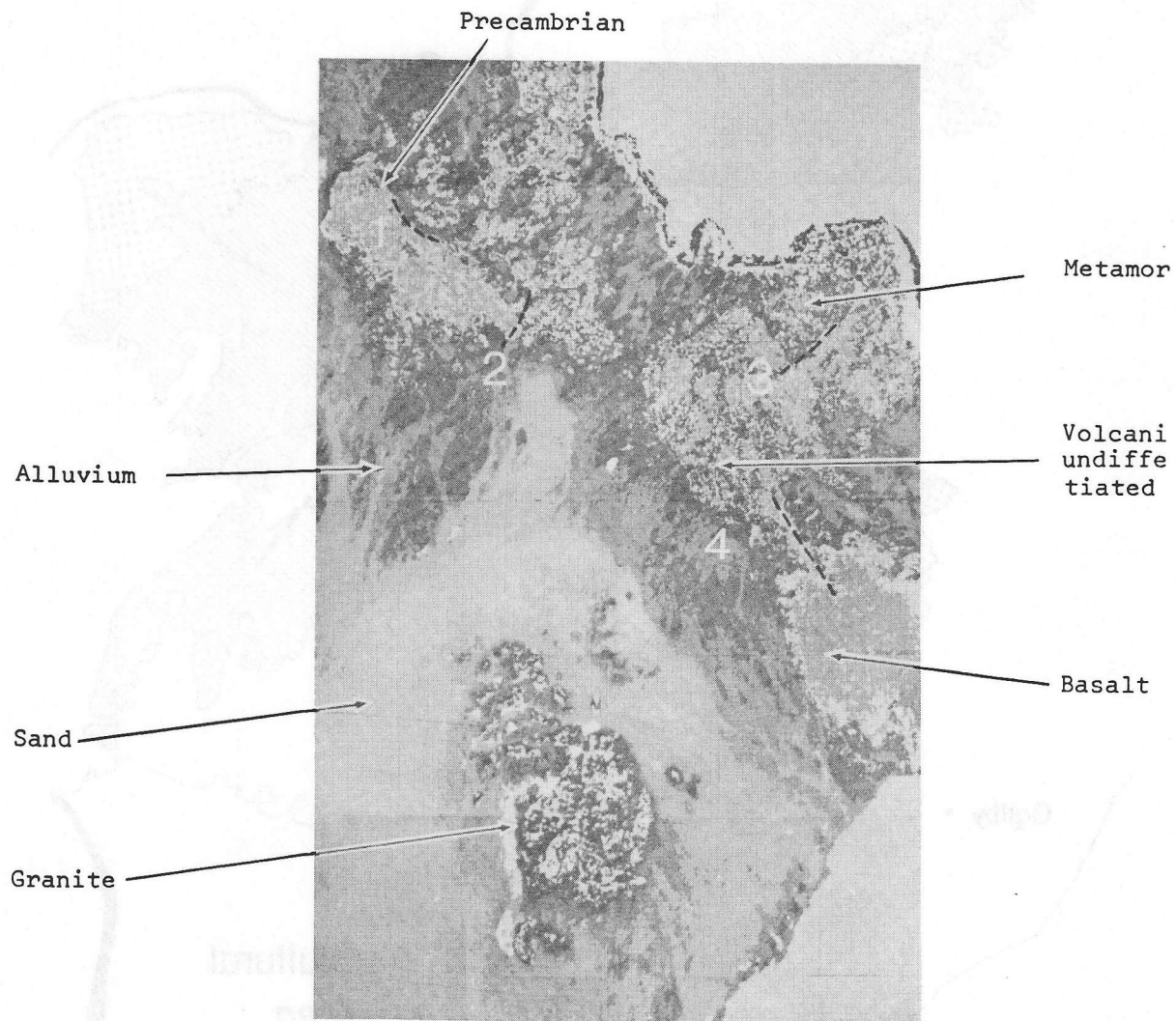


Figure 10. Computer Classification Map of Geological Features in Chocolate Mountains Area, California.